Chemical Anchoring of Palladium by Fe Oxo Ions in Zeolite ZSM-5

Bin Wen, Jifei Jia, and Wolfgang M. H. Sachtler*

V. N. Ipatieff Laboratory, Center for Catalysis and Surface Science, Department of Chemistry, Northwestern University, Evanston, Illinois 60208

Received: March 14, 2002; In Final Form: May 16, 2002

Zeolite supported mono- and bimetallic catalysts Pd/ZSM-5 and PdFe/ZSM-5 were prepared by exchanging Pd from a dilute aqueous solution of $[Pd(NH_3)_4](NO_3)_2$ into either H/ZSM-5 or Fe/ZSM-5. The Fe/ZSM-5 was prepared by sublimation; it contains a major part of the Fe as dinuclear oxygen-bridged Fe^{3+} ions. Significant differences between Pd/ZSM-5 and PdFe/ZSM-5 are revealed after calcination: in Pd/ZSM-5 the Pd is present as large PdO particles, but in PdFe/ZSM-5 it is highly dispersed over the zeolite cavities and invisible in TEM. Evidently, the Fe ions and/or Fe oxo ions act as very effective chemical anchors. It is argued that Pd^0 is formed by autoreduction of $[Pd(NH_3)_4]^{2+}$ ions even under calcination conditions. The Fe ions promote nucleation and limit growth of Pd^0_n clusters, which are subsequently converted to PdO.

1. Introduction

Pd/ZSM-5 is an active catalyst for the selective reduction of NO by CH_4 in the presence of O_2. There is some debate as to whether the active sites are Pd^{2+} ions,[1−3] PdO[4] or Pd^0 clusters, or (hydr)oxo ions such as $[Pd-O-Pd]^{2+}$ [5,6] or $H^+(PdO)H^+$,[7,8] but there is agreement that high and stable Pd dispersion is desirable for high catalytic activity. With conventional preparation techniques a significant fraction of the Pd will accumulate at the external surface of the zeolite, during either calcination or use as a catalyst, in particular for high loadings of Pd.[1,9] A clear incentive exists for the preparation of highly dispersed Pd/zeolite catalysts with high Pd loading that remains stable also during extended use. In the present study this is achieved by chemical anchoring of the Pd to the walls of the zeolite cavities.

Yermakov and Kuznetsov[10] prepared bimetallic clusters on silica by using Mo ions as the anchor. For instance, in Pt−Mo/SiO_2 prepared by reduction of Mo (π-$C_3H_5)_4$ complexes, the Pt is thought to be fixed on the SiO_2 surface by a Mo ion. Likewise, our group showed that the dispersion of platinum or rhodium in zeolite Y can be markedly improved by transition metal cations, such as Fe^{2+}.[11] More recently it was found that Fe/ZSM-5 with an Fe/Al atomic ratio of unity can be prepared by subliming $FeCl_3$ vapor onto H−ZSM-5.[12] After exchanging Cl by OH groups and calcination, a major portion of the Fe is present in such catalysts as an oxygen-bridged binuclear iron ion $[HO-Fe-O-Fe-OH]^{2+}$, as follows from CO-TPR, H_2-TPR, and ESR data. This model was recently confirmed by EXAFS and XANES results.[13,14]

In this paper we report on the effect of iron (oxo) ions on the dispersion of Pd in the same zeolite after calcination. FTIR, H_2-TPR, XRD, TEM, and EDX have been combined to characterize the catalysts. The conversion of $[Pd(NH_3)_4]^{2+}$ ions to Pd^0 and PdO during calcination of the catalyst precursor was followed by on-line mass spectrometry.

* Corresponding author. Telephone: (847) 491-5263. Fax: (847) 467-1018. E-mail: wmhs@northwestern.edu.

2. Experimental Section

2.1. Preparation of Samples. H/ZSM-5 was obtained by 3-fold ion exchange Na/ZSM-5 (Si/Al = 23, UOP) with a diluted NH_4NO_3 solution at ambient temperature, followed by calcination of the NH_4^+ form of the zeolite in an ultrahigh purity (UHP) O_2 flow at 550 °C for 4 h. Sublimation of $FeCl_3$ in an Ar flow at 320 °C was used by directing the vapor onto the heated H/ZSM-5. The detailed procedure is described in ref 12. After hydrolysis, the slurry was vacuum filtered, and the solid was washed thoroughly with doubly deionized (DDI) water, dried at 120 °C in air, and calcined in O_2 at 550 °C. This sample will be called Fe/ZSM-5. It has an Fe/Al ratio near unity.

To prepare Pd/ZSM-5 or PdFe/ZSM-5, a dilute solution (0.01 M) of $[Pd(NH_3)_4](NO_3)_2$ (Strem Chemical) was added dropwise to an H/ZSM-5 or Fe/ZSM-5 slurry at room temperature. After stirring for 72 h and filtering, the solid was washed with doubly deionized H_2O and air-dried, followed by calcination in a flow of pure O_2 (40 mL/min) of 1 atm. The temperature was ramped at 0.5 °C from room temperature to the 550 °C and then held at this temperature for 4 h. Elemental analysis via inductively coupled plasma spectroscopy (ICP) gives the following compositions in atomic ratios relative to Al:

Fe/ZSM-5: Na/Al = 0, Si/Al = 23, Fe/Al = 1.06

Pd/ZSM-5: Na/Al = 0, Si/Al = 23, Pd/Al = 0.20

PdFe/ZSM-5: Na/Al = 0, Si/Al = 23, Fe/Al = 1.07, Pd/Al = 0.18

2.2. Fourier Transform Infrared Spectra (FTIR). Infrared spectra were obtained with a Nicolet 60 SX FTIR spectrometer equipped with a liquid N_2 cooled mercury cadmium telluride (MCT) detector. Samples were pressed into 10 mg self-supporting wafers with a diameter of 13 mm. The wafers were inserted into a quartz cell sealed with NaCl windows connected to the gas manifold. They were calcined in situ for 1 h at 450 °C in an O_2 flow of 100 mL/min and cooled to room temperature in the same flow. All spectra were recorded at room temperature; 64 scans were accumulated with a spectral resolution of 1 cm^{-1}.

10.1021/jp020724s CCC: $22.00
Published on Web 07/03/2002

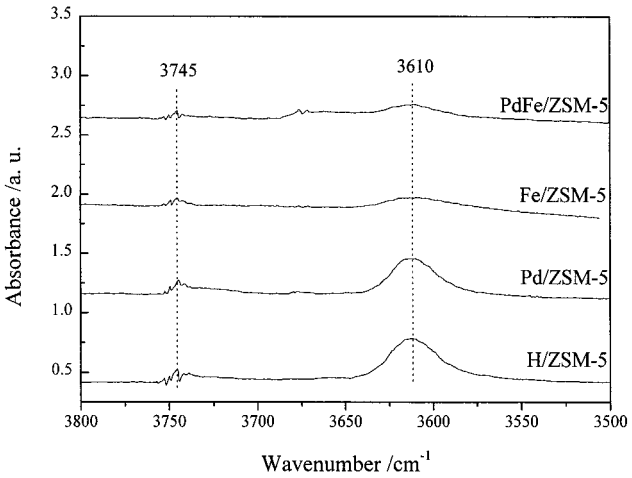

Figure 1. FTIR spectra in the OH stretching region of H/ZSM-5, Pd/ZSM-5, Fe/ZSM-5, and PdFe/ZSM-5.

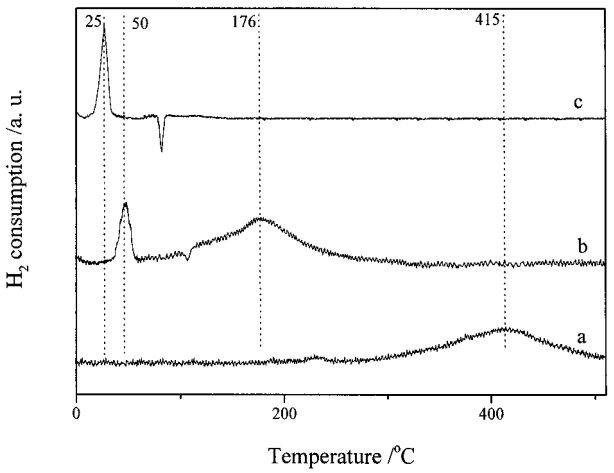

Figure 2. TPR profiles of (a) Fe/ZSM-5, (b) PdFe/ZSM-5, and (c) Pd/ZSM-5.

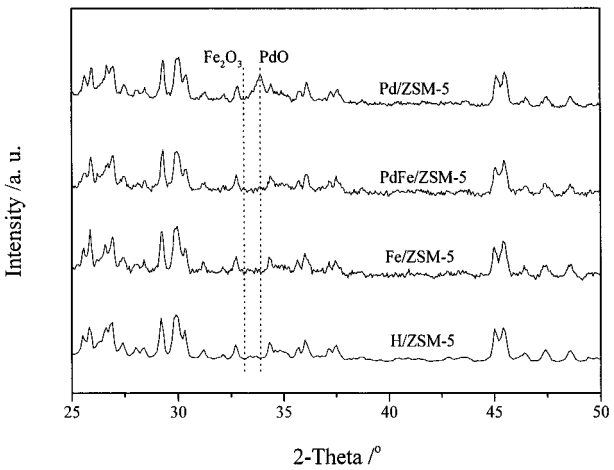

Figure 3. XRD patterns of H/ZSM-5, Fe/ZSM-5, PdFe/ZSM-5, and Pd/ZSM-5.

2.3. Temperature-Programmed Reduction (TPR). H_2-TPR was performed with an H_2/Ar (5%) flow of 40 mL/min from −80 to 600 °C with a ramp of 8 °C/min. The samples (50 mg) were pretreated for 1 h at 550 °C in pure O_2. The H_2 consumption was determined by a TCD detector, with H_2O being trapped in a dry ice-cooled trap. CuO/SiO_2 (quartz) was used as a standard to calibrate the consumption of H_2.

2.4. X-ray Diffraction (XRD). XRD patterns were recorded on a Rigaku diffractometer using Cu Kα radiation at 40 kV and 20 mA. Step-scan data were recorded from $2\theta = 10$ to 70° with a 0.02° step and 10 s counting time.

2.5. Transmission Electron Microscopy (TEM) and Energy Dispersive X-ray Analysis (EDX). A Hitachi HF-2000 cold field emission gun transmission electron microscope (FEG-TEM) equipped with an energy-dispersive X-ray (EDX) analyzer was used to obtain micrographs and compositions of selected particles. Samples were dispersed in ethanol. Approximately 1−2 μL of the suspension was pipetted onto a carbon-stabilized copper grid and dried in air. The TEM was operated at 200 keV accelerating voltage.

2.6. Temperature-Programmed Calcination of $[Pd(NH_3)_4]^{2+}$-Loaded Zeolite. The $[Pd(NH_3)_4]^{2+}$-loaded catalyst precursors were heated in a continuous flow (40 mL/min) of pure O_2 of 1 atm in a quartz reactor, while the temperature was increased linearly with a ramp of 0.5 °C/min. The gas products were monitored on-line by a Dycor M200 quadruple mass spectrometer. The monitored *m*/*e* values (ions) were 2 (H_2^+), 17 (OH^+, NH_3^+), 18 (H_2O^+), 28 (N_2^+), 30 (NO^+), 32 (O_2^+), 44 (N_2O^+), and 46 (NO_2^+).

3. Results

IR spectra in the hydroxyl stretching region are shown in Figure 1. With H/ZSM-5, a weak band at 3745 cm^{-1} and a strong band at 3610 cm^{-1} are attributed to isolated and terminal silanol groups[15] and acidic bridging hydroxyl groups,[16] respectively. For calcined Pd/ZSM-5, the presence of Pd has no obvious effect on the amount of Brønsted acid sites, indicating that in this stage, most Pd is present as uncharged PdO. In Fe/ZSM-5, the band at 3610 cm^{-1} is very weak, showing that most of the Brønsted acid sites have been replaced by Fe (oxo) ions. Introduction of Pd into Fe/ZSM-5 does not affect the OH bands, indicating that Pd in PdFe/ZSM-5 is not present as a positively charged entity.

Figure 2 shows the TPR profiles of freshly calcined Pd/ZSM-5, Fe/ZSM-5, and PdFe/ZSM-5 at the same scale. In Figure 2a, the broad peak centered at 415 °C corresponds to the reduction of the bridging oxygen in $[(HO)Fe-O-Fe(OH)]^{2+}$ to $[(HO)Fe-\square-Fe(OH)]^{2+}$. For Pd/ZSM-5, the sharp peak at 25 °C is ascribed to reduction of PdO particles. This assignment is confirmed by the absence of this peak in the sample that was prereduced with CO at 400 °C. The negative peak near 82 °C is characteristic of the decomposition of the Pd-β-hydride.[5] The presence of Pd in PdFe/ZSM-5 clearly enhances the reduction of the Fe^{3+} oxo ions significantly, the TPR peak is shifted from 415 °C in Fe/ZSM-5 to 176 °C in PdFe/ZSM-5. The PdO reduction peak is shifted upward by 25 °C with respect to Pd/ZSM-5. It is also noteworthy that the negative peak becomes very small and shifts to higher temperature.

XRD patterns are shown in Figure 3. No iron oxide phase is detected in Fe/ZSM-5 or PdFe/ZSM-5. A strong peak at $2\theta = 33.9°$ with Pd/ZSM-5 is typical for the (101) diffraction of PdO, indicating the presence of large PdO particles. Remarkably, this peak is absent in PdFe/ZSM-5, showing a much smaller PdO particle size in that sample. The peak at $2\theta = 40°$ known to be indicative for the (111) plane of Pd metal is absent in all samples. No significant changes in the XRD pattern of the zeolite are caused by the presence of the palladium.

More direct evidence regarding the sizes of the PdO particles in Pd/ZSM-5 and PdFe/ZSM-5 is obtained from the TEM and EDX results shown in Figure 4. The TEM micrograph of calcined PdFe/ZSM-5 in Figure 4a shows no visible particles in this sample, indicating a very high dispersion of PdO with

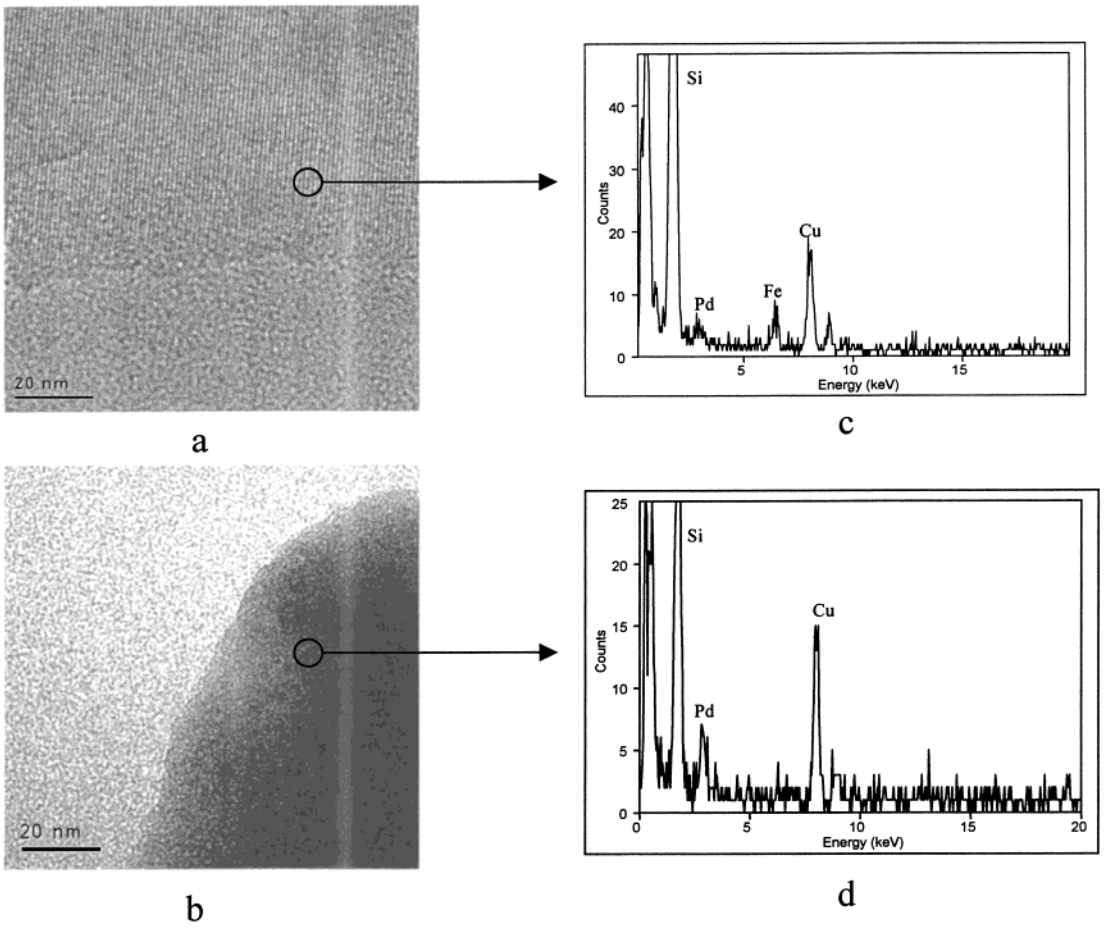

Figure 4. Representative TEM picture of (a) PdFe/ZSM-5, (b) Pd/ZSM-5, and relevant EDX spectra.

particle sizes on the same order as the zeolite channel diameters, i.e., 1−2 nm. EDX data of this sample, obtained by focusing on different areas of the TEM micrograph in Figure 4a, confirm the homogeneous distribution of the Pd. A representative example is shown in Figure 4c. Characteristic lines for both palladium and iron are clearly visible, indicating that Pd and Fe coexist inside zeolite cavities. In contrast, the TEM micrograph of calcined Pd/ZSM-5 in Figure 4b shows the presence of numerous particles of different sizes from 2 to 10 nm. Their chemical analysis by EDX (Figure 4d) identifies them as Pd. In the areas free of particles, no Pd signal is detected.

Temperature-programmed heating in oxygen of an uncalcined PdFe/ZSM-5 was monitored by on-line mass spectrometry. The profiles in Figure 5 show desorption of physisorbed H_2O near 107 °C. Oxidation of the ammine groups of the $[Pd(NH_3)_4]^{2+}$ ions is evident from the release of N_2, which starts at 165 °C and reaches two maxima located at 260 and 302 °C, respectively concomitant with the appearance of two maxima of H_2O at the same temperatures. The intensity ratio of the $m/e = 17$ and 18 indicates that the signal of $m/e = 17$ is due to the (OH^+) fragment ion of H_2O only; no intact NH_3 molecules are released. Likewise, no H_2 or NO_x are detected; N_2 and H_2O are the only products.

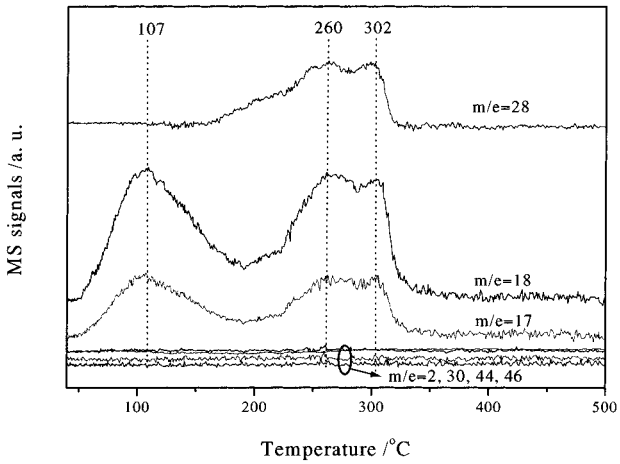

Figure 5. TPO patterns of an uncalcined PdFe/ZSM-5 sample. Temperature ramp 0.5 °C/min.

4. Discussion

The results show a dramatic change in Pd dispersion induced by the presence of Fe oxo ions in the zeolite. The present H_2-TPR, XRD, TEM, and EDX data indicate that after calcination of the catalyst precursor the PdO particles are homogeneously distributed throughout the zeolite channels in PdFe/ZSM-5, but large PdO particles illustrate inhomogeneous distribution of PdO particles in the case of Pd/ZSM-5.

Two paths can be visualized for the formation of PdO: (1) hydrolysis of Pd^{2+} ions to $PdO + 2H^+$ and (2) autoreduction of Pd^{2+} ions by ammine ligands, followed by oxidation. In either case the size distribution of the PdO particles will depend on the relative rates of the two basic phenomena: *nucleation* and *growth*. In the zeolite the growth rate is determined by the rate of migration of the precursors. If autoreduction of the Pd^{2+} ions by their ammine ligands takes place, the Pd^0 nuclei will grow when $Pd(NH_3)_n^{2+}$ ions ($n = 1$, 2, 3, or 4) are docking on them. Our previous work[17] indicates that in the absence of potential chemical anchors this is a fast process, because NH_3-ligated

Pd ions are highly mobile, in particular for $n = 2$, 3, or 4. If, however, hydrolysis takes place, the PdO particles can grow by coalescence with each other. The data in ref 18 indicate that this process is much slower. We therefore, assume that in Pd/ZSM-5 autoreduction of Pd by the NH_3 ligands, followed by trapping highly mobile $Pd(NH_3)_n^{2+}$ ions, is the prevailing process leading to large Pd particles that react subsequently with oxygen, thus becoming large PdO particles. These can coalesce, but the main cause of the formation of large particles is the high mobility of the $[Pd(NH_3)_n]^{2+}$ ions through the zeolite channels.

The presence of Fe thoroughly modifies this scenario: the rate of nucleation is dramatically increased, but the migration rate of the $Pd(NH_3)_n^{2+}$ ions toward these nuclei is decreased. The common cause of both phenomena is, of course, the overlap of d-orbitals in Fe and Pd. On the basis of studies of the proton spin relaxation time, Winkler et al.[19] suggested that Pt atoms which have not agglomerated will preferentially associate themselves with Fe^{3+} ions. Pt atoms are tightly bound to Fe^{3+} cations because the energy gained by polarization of the Pt atom in the electric field of an Fe^{3+} cation is greater than the dispersion energy by 2 orders of magnitude. In case some of the iron ions were reduced from Fe^{3+} to Fe^{2+} during autoreduction, a similar interaction between Fe^{2+} and Pd^0 exists, as suggested by Tzou et al. for Pt^0-Fe^{2+}.[11] For Rh/Al_2O_3, van Zon et al. showed that Rh−oxygen bonds linking the metal with the oxide support result in high dispersion of Rh.[20]

The chemical interaction of Pd, as Pd^0 atoms or Pd^{2+} ions, with Fe^{2+} and Fe^{3+} thus leads to a dramatic increase of the rate constant ratio k_{nucl}/k_{growth} and to a much higher dispersion of the Pd particles, which is retained also after the oxidation of Pd^0_n to $[PdO]_n$ particles.

Chemical anchoring of Pd^0 and Pt^0 by Fe^{2+} ions in zeolites has been reported before as a cause of high dispersion of Pd and Pt. In the present study, the effect appears more pronounced than in our previous work. The most likely cause for this is that the sublimation technique used in the present study leads to a much larger concentration of Fe^{3+} and Fe^{2+} ions than conventional ion exchange from aqueous solution. We cannot exclude, however, that the anchoring effect of oxygen-bridged Fe ions is intrinsically higher than that of isolated Fe ions.

As our IR data permit an estimate of the concentration of Brønsted acid sites in the zeolites also after calcination, the present study permits a comparison of the anchoring effects of Pd with either transition metal ions such as Fe or protons. Obviously, the formation of Pd−Fe bond has a much stronger effect on maintaining a high dispersion under the severe conditions of calcination than the mere formation of palladium−proton adducts.

Acknowledgment. This work was supported by the EMSI program of the National Science Foundation and the U. S. Department of Energy Office of Science (CHE-9810378) at the Northwestern University Institute for Environmental Catalysis. Financial aid from the Director of the Chemistry Division, Basic Energy Sciences, U. S. Department of Energy, Grant DE-FGO2-87ER13654, is gratefully acknowledged. We would like to thank Dr. Shuyou Li for his help in TEM and EDX data collection.

References and Notes

(1) Descorme, C.; Gélin, P.; Lécuyer, C.; Primet, M. *J. Catal*. **1998**, *177*, 352.
(2) Ogura, M.; Hayashi, M.; Kage, S.; Matsukata, M.; Kikuchi, E. *Appl. Catal. B* **1999**, *23*, 247.
(3) Ali, A.; Alvarez, W.; Loughran, C. J.; Resasco, D. E. *Appl. Catal. B* **1997**, *14*, 13.
(4) Okumura, K.; Amano, J.; Yasunobu, N.; Niwa, M. *J. Phys. Chem. B* **2000**, *104*, 1050.
(5) Wen, B.; Sun, Q.; Sachtler, W. M. H. *J. Catal*. **2001**, *204*, 314.
(6) Wen, B.; Sachtler, W. M. H. *Appl. Catal. A* **2002**, *230*, 11.
(7) Aylor, A. W.; Lobree, L. J.; Reimer, J. A.; Bell, A. T. *J. Catal* **1997**, *172*, 453.
(8) Lobree, L. J.; Aylor, W. A.; Reimer, J. A.; Bell, A. T. *J. Catal*. **1999**, *181*, 189.
(9) Gélin, P.; Goguet, A.; Descorme, C.; Lécuyer, C.; Primet, M. In *IVth International Congress On Catalysis and Automotive Pollution Control*, April 1997, Brussels, Vol. 2, p 197.
(10) Yermakov, Yu. I.; Kuznetsov, B. N. *J. Mol. Catal.* **1980**, *9*, 13.
(11) Tzou, M. S.; Jiang, H. J.; Sachtler, W. M. H. *Appl. Catal.* **1986**, *20*, 231.
(12) Chen, H.-Y.; Sachtler, W. M. H. *Catal. Today* **1998**, *42*, 73.
(13) Marturano, P.; Drozdová, L.; Kogelbauer, A.; Prins, R. *J. Catal*. **2000**, *192*, 236.
(14) Battiston, A. A.; Bitter, J. H.; Koningsberger, D. C. *Catal. Lett.* **2000**, *66*, 75.
(15) Zecchina, A.; Bordiga, S.; Spoto, G.; Marchese, L.; Petrini, G.; Leofanti, G.; Padovan, M. *J. Phys. Chem.* **1992**, *96*, 4991.
(16) Chester, A. W.; Dessan, R. M.; Alemani, L. B.; Woolery, G. L. *Zeolites* **1986**, *6*, 14.
(17) Homeyer, S. T.; Sachtler, W. M. H. *J. Catal*. **1989**, *117*, 91.
(18) Lebedeva, O. E.; Chiou, W.-A.; Sachtler, W. M. H. *J. Catal*. **1999**, *188*, 365.
(19) Winkler, H.; Ebert, A.; Ebert, W.; Riedel, E. *Surf. Sci*. **1975**, *50*, 565.
(20) van Zon, J. B. A. D.; Koningsberger, D. C.; van't Blik, H. F. J.; Sayers, D. E. *J. Chem. Phys.* **1985**, *82*, 44.